Applied Catalysis B: Environmental 111–112 (2012) 271–279

Contents lists available at SciVerse ScienceDirect

Applied Catalysis B: Environmental

journal homepage: www.elsevier.com/locate/apcatb

Synthesis, characterization and photocatalytic performance of novel visible-light-induced Ag/BiOI

Hong Liu [a,*], Weiran Cao [a], Yun Su [a], Yong Wang [a,*], Xiaohong Wang [b]

[a] Department of Chemical Engineering, School of Environmental and Chemical Engineering, Shanghai University, 99 Shangda Road, Shanghai 200444, PR China
[b] Institute of Nano Micro Energy, Shanghai University, 99 Shangda Road, Shanghai 200444, PR China

ARTICLE INFO

Article history:
Received 26 May 2011
Received in revised form
28 September 2011
Accepted 4 October 2011
Available online 12 October 2011

Keywords:
Ag/BiOI
Visible-light photocatalysis
Electron–hole separation
Dyes

ABSTRACT

For the first time, a series of Ag/BiOI photocatalysts with different Ag contents have been synthesized by a hydrothermal combinated with photodeposition method. The as-prepared products were characterized by powder X-ray diffraction (XRD), scanning electron microscopy (SEM), energy-dispersive X-ray spectroscopy (EDX), transmission electron microscopy (TEM), high-resolution transmission electron micrographs (HRTEM), X-ray photoelectron spectroscopy (XPS), UV–vis diffuse reflectance spectra (DRS), and photoluminescence (PL) emission spectroscopy. The photocatalytic activities of these Ag/BiOI composites under visible-light irradiation ($\lambda > 420$ nm) were evaluated by the degradation of acid orange II, methyl orange (MO) and rhodamine B (RB). The results revealed that the Ag/BiOI composites exhibited much higher photocatalytic activities than pure BiOI. The Ag amount in the Ag/BiOI composites played an important role in the corresponding photocatalytic properties and the optimized ratio was obtained at 0.6%. The significant enhancement in the Ag/BiOI photoactivity could be ascribed to both the effect of Ag deposits by acting as electron traps and the surface plasma resonance effect of Ag.

1. Introduction

In the past decades, semiconductor photocatalysts have attracted considerable attention due to their potential applications for solving energy and pollution problems [1–3]. Among the diverse photocatalytic materials, TiO_2 is mostly studied because of its chemical and biological inertness, high stability against photocorrosion, non-toxicity and low cost. However, TiO_2 can only be excited by UV irradiation ($\lambda < 380$ nm) due to its wide band gap, which is no more than 4% of the solar spectrum, severely rendering the overall process impractically [4]. Considering visible-light accounts for 43% of the solar spectrum, therefore, it is indispensable to develop visible-light-driven photocatalysts. Nowadays, two strategies have been employed in the design of visible-light-driven photocatalysts. One of the efforts is the modification of TiO_2, including nonmetal/metal doping, dye sensitization, coupling with other semiconductor, etc. [5–11]. However, little progress has been made in industrial application because the photocatalytic activity of modified TiO_2 is still very low under visible light radiation. Another strategy is the development of new semiconductor materials capable of absorbing visible light.

As V–VI–VII ternary oxide semiconductors, bismuth oxyhalides, BiOX (X = F, Cl, Br, I), have recently attracted much attention due to their remarkable photocatalytic activities in degradation of organic compounds [12–14]. They may serve as a new family of promising photocatalysts. All BiOX compounds possess better photocatalytic activity than TiO_2 (P25, Degussa) under UV illumination due to their particular layer structure characterized by $[Bi_2O_2]$ slabs interleaved by double slabs of halogen atoms [15]. However, due to their wide optical bandgap, BiOF and BiOCl can only absorb UV-light. In comparison, BiOBr and BiOI are both visible-light responsive. Among the bismuth oxyhalides, BiOI, with an estimated band gap of about 1.7 eV, is of particular importance because it possesses the strongest absorption in the visible-light region and the best photocatalytic activity [16].

Considering BiOI as a possible visible light responding photocatalyst, its photocatalytic efficiencies must be further improved in order to be suitable for practical applications. So it is very significant to modify the photocatalytic activity of BiOI by various methods. Recently, Wang and co-workers coupled BiOI with BiOBr and found that BiOBr–BiOI exhibited better performance than pure BiOI on photocatalytic degradation of methyl orange (MO) dye [12]. Zhang's group synthesized the BiOI/TiO_2 heterostructures, and 95% of MO could be degraded in 2 h over 50% BiOI/TiO_2 heterostructure while the BiOI is merely 2% [17].

Noble metal-modified semiconductor nanoparticles have become the focus of many studies for maximizing the efficiency of photocatalytic reactions in recent years [18]. It is believed that

* Corresponding authors. Tel.: +86 21 66137487; fax: +86 21 66137725.
E-mail addresses: liuhong@shu.edu.cn (H. Liu), yongwang@shu.edu.cn (Y. Wang).

0926-3373/$ – see front matter © 2011 Elsevier B.V. All rights reserved.
doi:10.1016/j.apcatb.2011.10.008

the metal deposition can act as traps for photoinduced electrons, leading to the reduction of electron–hole recombination [19]. Various metals such as Pt, Pd, Ag, Au, Rh have been utilized for increasing the photocatalytic activity of semiconductor oxides [20,21]. Among these noble metals, silver (Ag) is one of the most suitable for industrial applications due to its low cost and low toxicity. However, up to now no report has been made about the noble metal effects on the photocatalytic performance of oxyhalides.

Motivated by these facts, for the first time we developed a facile hydrothermal combinated with photodeposition method to prepare Ag/BiOI photocatalysts with high crystallinity. The prepared samples were characterized, and the photodegradations of acid orange II, methyl orange and rhodamine B (RB) were employed to evaluate the photocatalytic activities of Ag/BiOI photocatalysts under visible-light irradiation ($\lambda > 420$ nm). The results revealed that all Ag/BiOI photocatalysts exhibited much higher photocatalytic activity than the single-phase BiOI, while 0.6%Ag/BiOI possessed the best activity. The possible mechanism of photocatalytic activity enhancement and the effect of silver deposition were investigated on the basis of characterization results.

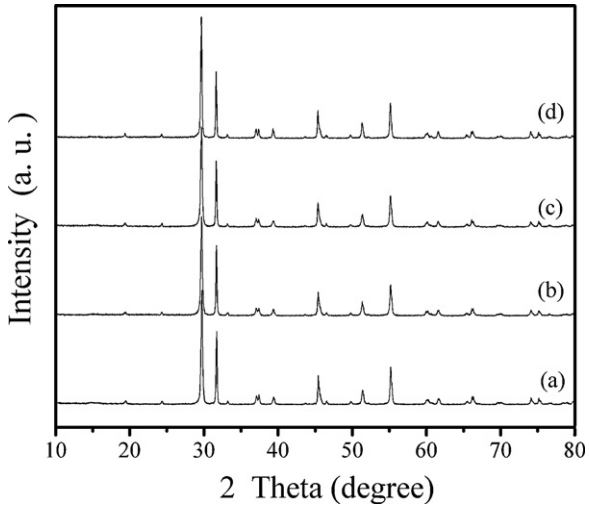

Fig. 1. XRD patterns of BiOI and Ag/BiOI powders: (a) BiOI, (b) 0.3%Ag/BiOI, (c) 0.6%Ag/BiOI and (d) 0.9% Ag/BiOI.

2. Experimental

2.1. Synthesis

The pure BiOI samples were synthesized by a hydrothermal method. All the reagents were purchased from the Sinopharm Chemical Reagent Co., Ltd. and were used without further purification. In a typical synthesis, 0.97 g $Bi(NO_3)_3{\cdot}5H_2O$ was firstly dissolved in 3 ml acetic acid (HAc). Then the solution was added slowly to 50 ml deionized water containing 0.30 g NaI under magnetically stirring. After stirring for 30 min at room temperature, the suspension was transferred into a Teflon-lined stainless steel autoclave (100 ml capacity). The autoclave was heated at 100 °C for 6 h under autogenously pressure, and then was cooled to room temperature naturally. The resulting precipitate was filtrated and washed with ethanol and deionized water thoroughly and then dried at 60 °C overnight in air. The powders were collected as the final product.

Ag/BiOI composites were prepared by a photoreduction method. Firstly, 0.80 g as-prepared BiOI powders were dispersed in 30 ml deionized water. Then 0.001 mol/l $AgNO_3$ with different volume and excess methanol as the electron donor were added. After being stirred for 1 h in the dark, the suspensions were irradiated with UV light (500 W mercury lamp) for 4 h with continual stirring. The color of the reaction mixture was observed to change from red to red-brown, indicating the reduction and the deposition of Ag on BiOI. Finally, the product was centrifuged, washed with distilled water and dried at 100 °C for 24 h. The catalyst loaded with *x*% (wt) Ag was denoted as *x*% Ag/BiOI.

2.2. Characterization

The crystalline phases of the catalysts were evaluated by X-ray diffraction (XRD, D/MAX-2550, Cu K, $\lambda = 0.15418$ nm). The morphologies and microstructures of prepared samples were analyzed by scanning electron microscope (SEM, JSM-6700F) equipped with an energy-dispersive X-ray spectroscopy (EDX) system, transmission electron microscopy (TEM) (JEOL 200CX) and high-resolution transmission electron microscopy (HRTEM)(JEM-2010F). The absorption properties of the samples were obtained on an UV–vis spectrophotometer (Hitachi U-3010) using $BaSO_4$ as a reference. To study the recombination of photo-induced charge carrier, photoluminescence (PL) spectra were measured using a Hitachi F-7000 fluorescence spectrophotometer at room temperature. The surface compositions of the catalysts were evaluated by X-ray photoelectron spectra (XPS, PHI ESCA-5000C).

2.3. Photocatalytic activity test

Photocatalytic activities of the samples were evaluated by the photocatalytic degradation of different dyes (acid orange II, MO and RB) in an aqueous solution under visible-light irradiation. The photocatalytic system included a 500 W Xe arc lamp with a UV cutoff filter ($\lambda > 420$ nm), circulation of water through an external cooling coil and a ventilating fan, which were used to prevent any thermal catalytic effects. All experiments were conducted at room temperature in air. In a typical photocatalytic experiment, 0.05 g of the photocatalyst was added into 50 ml of 10 mg/L dyes solution in a reaction cell with a Pyrex jacket. Prior to irradiation, the suspension was magnetically stirred in the dark for 1 h to reach an adsorption–desorption equilibrium of the dyes on the catalyst surface. Then the suspension was exposed to visible-light irradiation under magnetic stirring. At given time intervals, about 5 ml suspensions were collected and centrifuged (13,000 rpm, 15 min) to remove the photocatalyst particles. Then the dye concentration of the obtained solution was analyzed by a UV–vis spectrophotometer (Hitachi, U-3310) by checking the absorbance at 485 nm, 464 nm and 553 nm for acid orange II, MO and RB, respectively.

3. Results and discussion

3.1. Crystal structure

Fig. 1 shows the XRD patterns of the as-prepared samples. All the reflections can be readily indexed to the characteristic peak of tetragonal BiOI [JCPDS file No.10-0445]. No impurities can be detected from the pattern of BiOI, which indicates that well-crystallized BiOI can be prepared by the hydrothermal process. In addition, there is no any diffraction peak of silver species (38.1°, 44.2°, 64.4°, and 77.4° for Ag (0) [22] and 34.2° for Ag (I) [23]) can be observed for the silver deposited samples, suggesting that all the prepared photocatalysts possess the same crystal structure. This may be attributed to the low concentration of silver (0.3 –0.9 wt%).

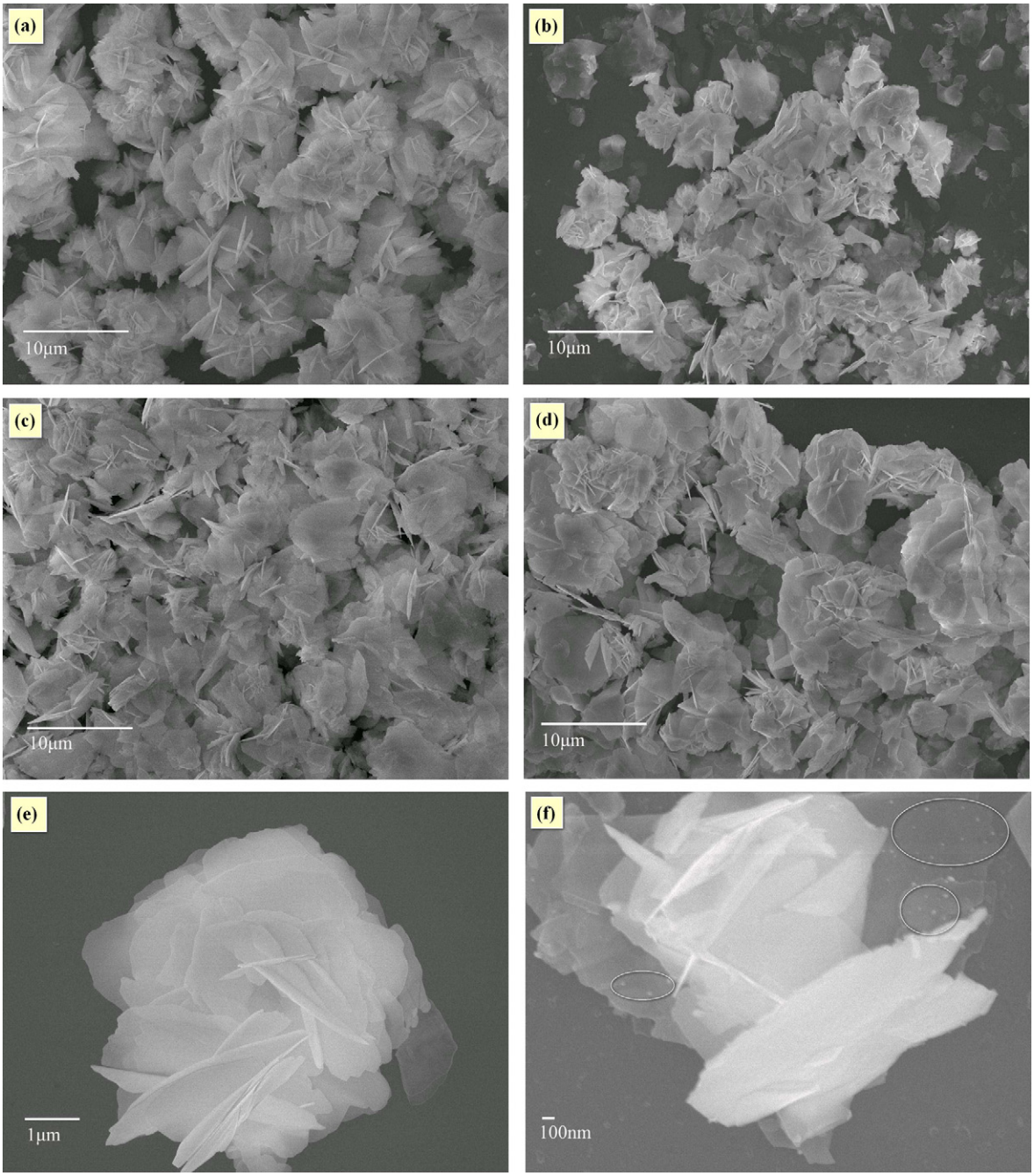

Fig. 2. Low-magnification SEM images of BiOI and Ag/BiOI: (a) BiOI, (b) 0.3% Ag/BiOI, (c) 0.6%Ag/BiOI, (d) 0.9% Ag/BiOI and high-magnification SEM images: (e) BiOI and (f) 0.6%Ag/BiOI.

3.2. Morphology and microstructure

Fig. 2 shows the SEM images of the pure BiOI and Ag/BiOI samples. As shown in Fig. 2a, the pure BiOI has a uniform, flower-like architecture with the diameter of approximately 6–10 μm. The flower-like architecture is composed of numerous irregular nanopetals (Fig. 2e). All the Ag/BiOI samples are of the similar morphology to BiOI, which can be observed in Fig. 2b–d, indicating silver doping through photoreduction did not significantly affect the morphology of BiOI. The high-magnification SEM image of 0.6%Ag/BiOI (Fig. 2f) shows that lots of Ag nanoparticles (marked by circles) are dispersed on the edges of BiOI lamellas. EDX analysis of 0.6%Ag/BiOI shows that the sample is composed of Bi, O, I and Ag atoms (Fig. 3). Quantitative analysis shows that the atomic ratio of Bi/O/I is 1:2.07:1.10, indicating the product is oxygen-rich. The excess oxygen might arise from the surface OH and adsorbed H_2O [24]. In addition, the Ag content is 0.68% (wt) obtained from EDX, which approximates the theoretical value.

Fig. 4 displays the TEM and HRTEM images of the as-synthesized 0.6%Ag/BiOI. As presented in Fig. 4a, the morphology of the sample is composed of large lamellar structure, and lots of the pleats prove that the lamellas are ultrathin. Moreover, some small metallic Ag nanoparticles (marked by arrow), with diameter about 10–20 nm, can be clearly observed. This agrees well with the SEM observation. There are no isolated Ag nanoparticles or Ag aggregates found in TEM observations, indicating that all metallic Ag nanoparticles are completely and evenly dispersed on BiOI samples. The HRTEM image of 0.6%Ag/BiOI shown in Fig. 4b reveals that the materials are

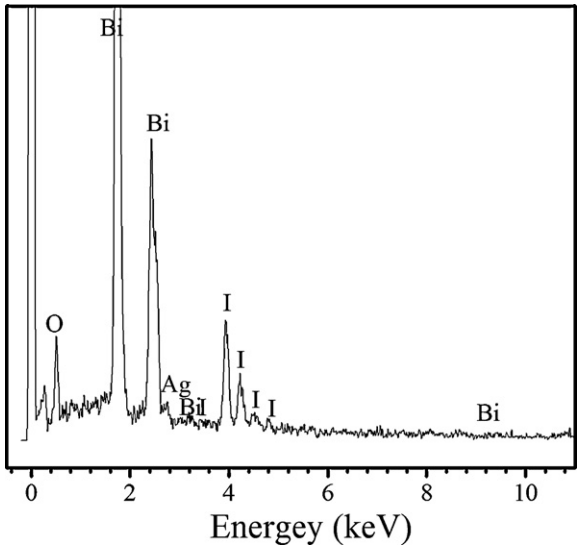

Fig. 3. EDX spectrum of the 0.6%Ag/BiOI sample.

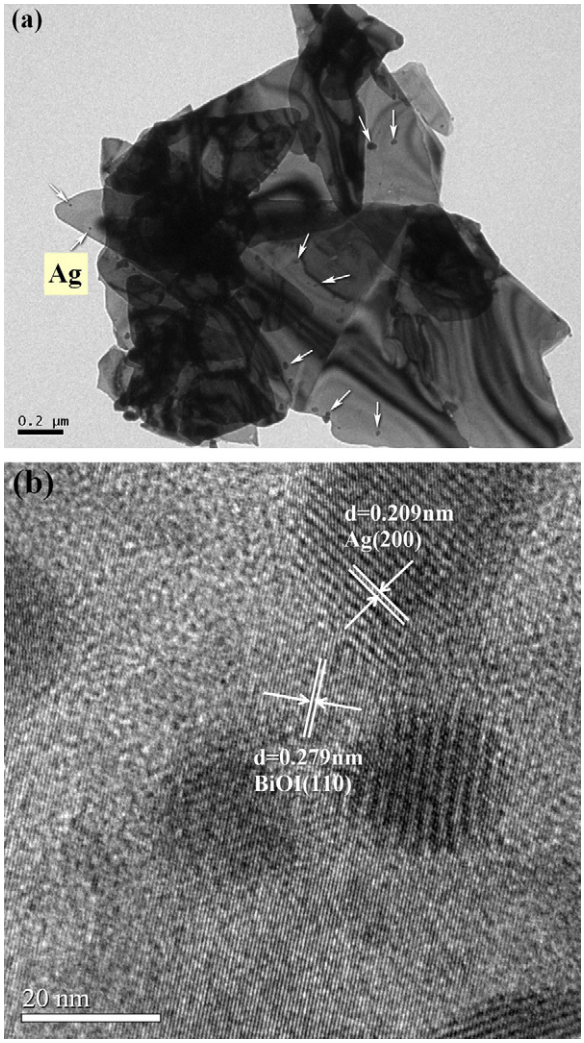

Fig. 4. TEM (a) and HRTEM (b) images of 0.6%Ag/BiOI.

highly crystallized, as evidenced by well-defined lattice fringes. The lattice spacings are about 0.209 and 0.279 nm, corresponding to the (2 0 0) plane of Ag and the (1 1 0) plane of tetragonal BiOI, respectively. Fig. 4b also suggests that the Ag nano-grains are embedded in the BiOI matrix. This clearly indicates that a tight heterojunction has been formed between BiOI and Ag in a nano-size level.

3.3. XPS spectra

The surface chemical states of 0.6%Ag/BiOI powder were also investigated by XPS analysis. Fig. 5a is a typical XPS survey spectrum of different atoms. The binding energies of different atoms were determined by internally referencing the adventitious carbon at a binding energy of 284.8 eV. Fig. 5a shows that the Ag/BiOI powder is composed of Bi, O, I and Ag and a trace amount of C. The C element is ascribed to the adventitious hydrocarbon from XPS instrument itself. Fig. 5b shows the high-resolution XPS spectrum of the Bi 4f. The peaks with binding energy of 158.6 and 163.9 eV are for the Bi $4f_{7/2}$ and Bi $4f_{5/2}$ respectively, which is characteristic of Bi^{3+} in BiOI. The satellite peaks are at 1.0 eV away from Bi $4f_{7/2}$ and Bi $4f_{5/2}$ main peaks, corresponding to the reported values [25]. In Fig. 5c, the O 1s core level spectrum can be fitted into three peaks at 529.6, 530.9 and 532.1 eV, indicating three different kinds of O species in the sample. The dominant peak at 529.6 eV is attributed to the Bi–O bonds in $[Bi_2O_2]$ slabs of BiOI [26]. The other two peaks at around 530.9 and 532.1 eV suggest the presence of other components such as OH, H_2O and carbonate species adsorbed on the surface [27]. The XPS spectrum of I 3d core is shown in Fig. 5d. The peaks at binding energies of around 630.1 eV (I $3d_{3/2}$) and 618.7 eV (I $3d_{5/2}$) can be ascribed to pure BiOI, which indicates that the state of I in the sample is −1 valence [28]. The peaks centered at 368.1 eV and 374.1 eV in Fig. 5e correspond to Ag $3d_{5/2}$ and Ag $3d_{3/2}$ [29], respectively, and the slitting of the 3d doublet is 6.0 eV. Previous studies on the XPS show that the Ag $3d_{5/2}$ binding energies for the Ag, Ag_2O and AgO are 368.2 eV, 367.8 eV and 367.4 eV, respectively [30,31]. Therefore, it is confirmed that Ag mainly exists in the Ag (0) state [32,33]. And Ag species may be merely dispersed on the surface of BiOI crystal without doping into the crystal lattice.

3.4. UV–vis diffuse reflectance spectra and band gap

Fig. 6 reveals that all samples exhibit strong absorptions in the visible light region. It is apparent that the absorption edges of all the samples loaded with Ag show the slight red-shift. And with the increase of Ag content, the absorption becomes stronger in the visible range. These may be attributed to the surface plasma resonance (SPR) effect of spatially confined electrons in metallic Ag nanoparticles [34–36]. It is suggested that the visible-light-responses of Ag/BiOI composites are significantly improved by the Ag doping and therefore it should have better photoactivity than the pure BiOI.

The band gap energy of a semiconductor can be calculated by the following formula:

$$\alpha h\nu = A(h\nu - E_g)^{n/2} \quad (1)$$

where α, h, ν, E_g, and A are the absorption coefficient, Planck constant, the light frequency, the band gap, and a constant, respectively. Among them, n depends on the characteristics of the transition in a semiconductor, i.e., direct transition ($n = 1$) or indirect transition ($n = 4$). For BiOI, the value of n is 4 for the indirect transition [26]. Therefore, the band gap energy (E_g value) of the resulting samples can be estimated from a plot $(\alpha h\nu)^{1/2}$ versus photon energy ($h\nu$). The intercept of the tangent to the X axis would give a good approximation of the band gap energy of the samples (Fig. 7).

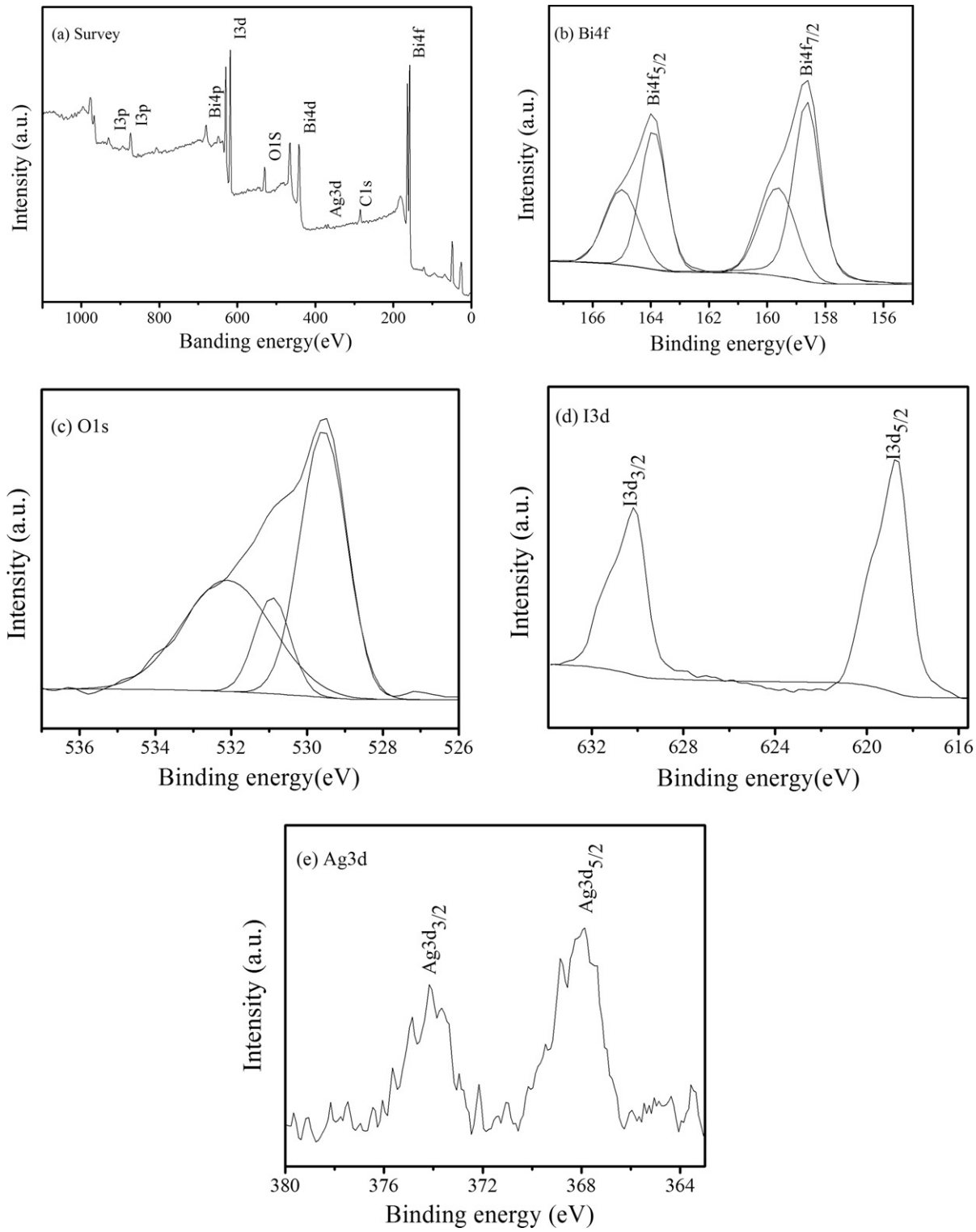

Fig. 5. XPS spectra of 0.6%Ag/BiOI powder: (a) survey spectrum, (b) Bi 4f, (c) O 1s, (d) I 3d and (e) Ag 3d.

Their calculated band gap energies are summarized in Table 1. The band gap of BiOI is evaluated to be 1.72 eV, close to the values reported in the literature [16,37]. It is found that the band gap of Ag/BiOI powders ranges from 1.70 to 1.66 eV and decreases with the increased Ag content from 0.3 to 0.9%. These results also support that all these samples have suitable band gaps, which is able to be activated by visible-light for photocatalytic decomposition of organic contaminants.

Table 1
Band gaps, valence band and conduction band of as-prepared samples.

Catalyst	Bandgap, E_g (eV)	Valence band, E_{VB} (eV)	Conduction band, E_{CB} (eV)
BiOI	1.72	2.35	0.63
0.3%Ag/BiOI	1.70	2.34	0.64
0.6%Ag/BiOI	1.68	2.33	0.65
0.9%Ag/BiOI	1.66	2.32	0.66

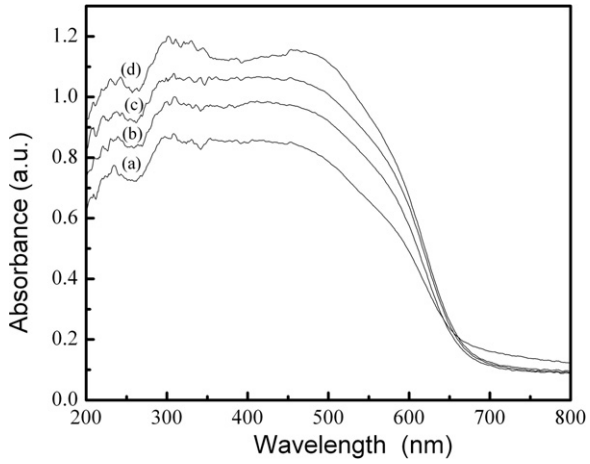

Fig. 6. Diffuse reflectance spectra of the catalysts: (a) Pure BiOI, (b) 0.3% Ag/BiOI, (c) 0.6% Ag/BiOI and (d) 0.9% Ag/BiOI.

3.5. PL properties

The PL technique can reflect the recombination rate of the photoinduced electrons and holes, which are useful to evaluate the photocatalytic performance of the semiconduct materials [38]. In Fig. 8, two emitting peaks, at around 587 nm and 602 nm are observed for pure BiOI sample when excited by 390 nm laser. The energy of used excitation light is enough to promote electronic transitions from the VB to the CB of BiOI according to the above DRS spectrum (Fig. 6). Though shapes and peaks positions of Ag/BiOI samples are similar to the pure BiOI, the emission intensity of the as-synthesized Ag/BiOI decreases. In addition, the emission band intensities of the spectra vary for the different doping amounts of silver. The optimal Ag content (0.6%) caused the biggest decrease in the intensity of the photoluminescence peak. It is known that the photoluminescence spectrum of semiconductor can be attributed to the radiative recombination process of self-trapped excitations. Therefore, the presence of Ag can suppress the radiative recombination process, leading to weak recombination of the e^-/h^+ pairs and high photon efficiency. This effect is also related to the concentration of silver, the high doping level (0.9%) may lead to some new recombination centers and the decrease of this effect.

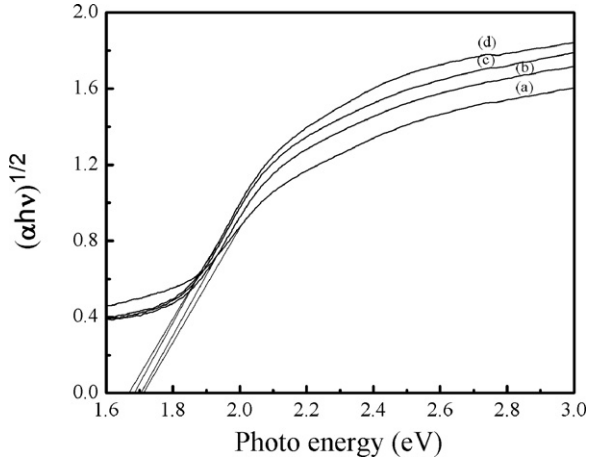

Fig. 7. Plots of the $(\alpha h\nu)^{1/2}$ vs photon energy ($h\nu$) for as-synthesized samples: (a) BiOI, (b) 0.3%Ag/BiOI, (c) 0.6%Ag/BiOI and (d) 0.9%Ag/BiOI.

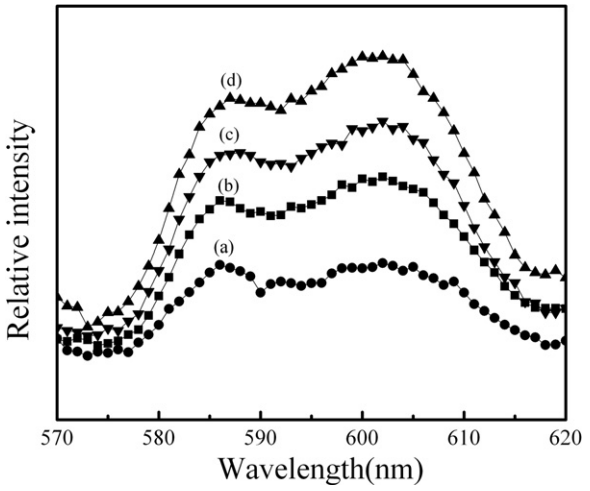

Fig. 8. PL spectra of the as-synthesized samples: (a) 0.6%Ag/BiOI, (b) 0.3%Ag/BiOI, (c) 0.9%Ag/BiOI and (d) BiOI.

3.6. Photocatalytic activity

The photocatalytic activities of as-prepared samples were evaluated by measuring the degradation of acid orange II, MO and RB in an aqueous solution under visible light. It is well known that there are three possible mechanisms for dye photodegradation: a photolysis process, a dye photosensitization process and a photocatalytic process. In order to investigate the mechanisms, the degradation of the three dyes in the absence of photocatalyst and presence of P25 under visble light were also studied. Fig. 9a–c shows that the three dyes photolysis in the blank experiment are not observable and a slight degradation of acid orange II, MO and RB over P25, which indicate that the three dyes have high structural stability and the photolysis as well as the dye-sensitive process are neglectable. Therefore, in our experiment, the mechanism for dyes degradation is a photocatalytic process.

Fig. 9a exhibits the photocatalytic activities of different catalysts in the degradation of acid orange II under visible light irradiation. It can be seen that the acid orange II degradation over pure BiOI is 47.8% after 4 h of visible-light irradiation. Compared to this, the Ag deposition has a significant influence. It is observed that the photocatalytic efficiency increases with the increased Ag from 0 to 0.6 wt%, but with the further increase from 0.6 to 0.9 wt%, the photocatalytic activity decreases. When the deposition is 0.6%, the catalytic activity is up to 92.1%. More Ag contents could be detrimental to the photonic activity. Fig. 9b and c displays the photodegradation of MO and RB as a function of irradiation time. After irradiation for 4 h, about 31.3% of MO and 17.8% of RB are decomposed for BiOI. In comparison, the Ag/BiOI composites show much better activity than pure BiOI and the optimal deposited content of silver is found to 0.6%. For 0.6%Ag/BiOI, the MO and RB removal efficiency reaches 80.0% and 49.6%, respectively.

To quantitatively understand the reaction kinetics of the dye degradation, the pseudo-first-order model as expressed by Eq. (2) was used to analyze the photocatalytic degradation data if the initial concentration of pollutant is low:

$$\ln\left(\frac{C_0}{C}\right) = kt \tag{2}$$

where C_0 and C are the concentrations of dye at time 0 (the time to obtain adsorption-desorption equilibrium) and t, respectively, and k is the pseudo-first-order rate constant. The rate constants evaluated from the data plotted in Fig. 9a, b and c are also summarized in Table 2. It can be seen, a fairly good correlation to the pseudo-first-order reaction kinetics ($R > 0.96$) is found. The rate constant

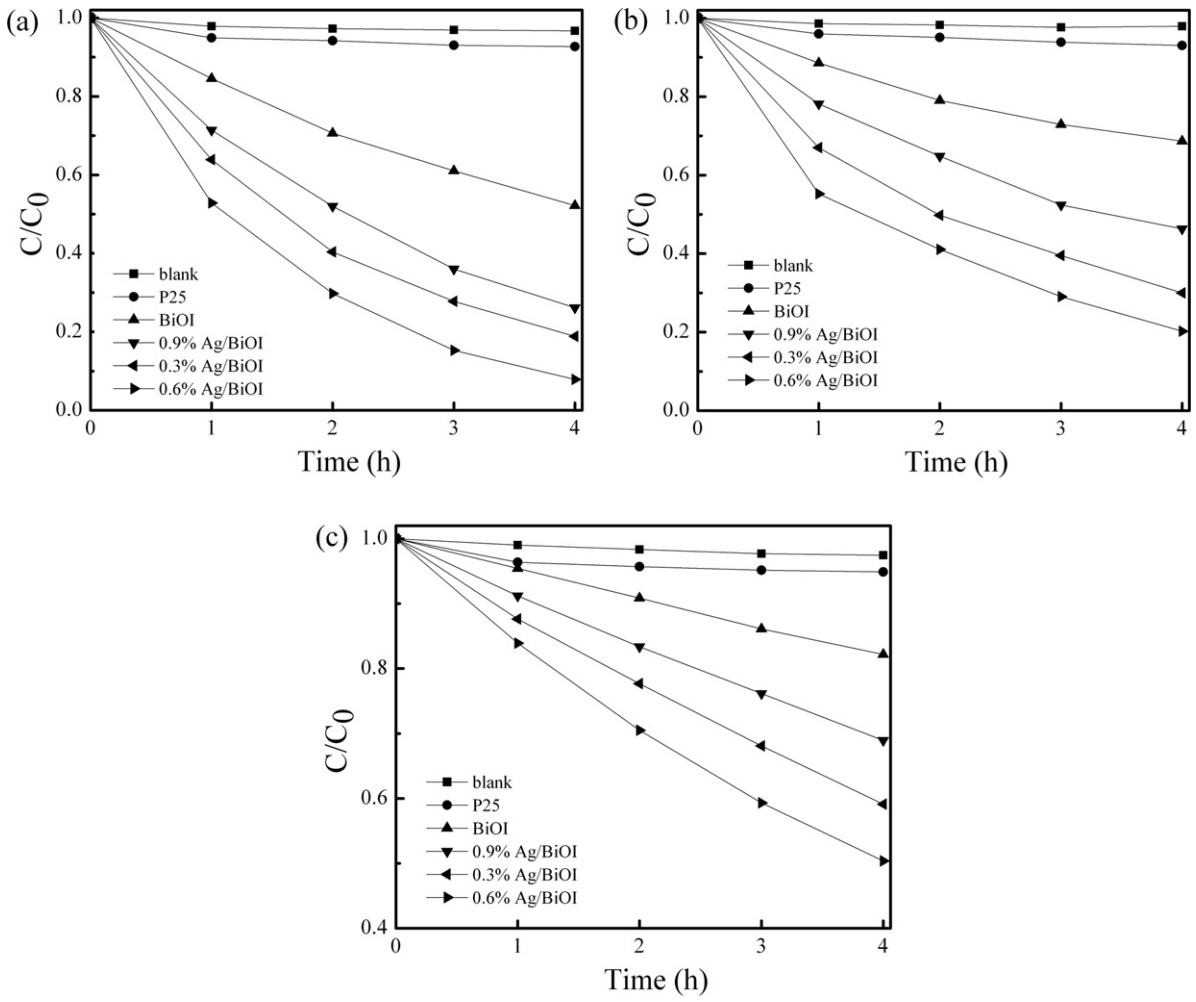

Fig. 9. Photocatalytic activities of BiOI and Ag/BiOI samples on the degradation of dyes under visible-light irradiation. (a) acid orange II, (b) MO, (c) RB.

of 0.6%Ag/BiOI is about 4.00, 3.99 and 3.39 times of that of BiOI in degradation of acid orange II, MO and RB, respectively. These suggest that Ag/BiOI is a much more effective photocatalyst than pure-phase BiOI due to Ag deposition.

The valance band (VB) of a photocatalyst is an important factor for the effective photocatalytic decomposition of organic contaminants [39]. The valence band edge position of Ag/BiOI was estimated in this work according to the concepts of electronegativity. Herein, the electronegativity of an atom is the arithmetic mean of the atomic electron affinity and the first ionization energy [40]. The valence band potentials of a semiconductor at the point of zero charge can be calculated by the following empirical equation [41]:

$$E_{VB} = X - E^e + 0.5E_g \quad (3)$$

where E_{VB} is the VB edge potential, X is the electronegativity of the semiconductor, which is the geometric mean of the electronegativity of the constituent atoms, E^e is the energy of free electrons on the hydrogen scale (about 4.5 eV), E_g is the band gap energy of the semiconductor, the X value of BiOI is ca. 5.99 eV, and E_{CB} can be determined by $E_{CB} = E_{VB} - E_g$. The E_{VB} and E_{CB} of the samples are calculated and have been summarized in Table 1. It is obvious that all of the valence band (VB) edge potentials of as-prepared photocatalysts are more positive than the standard redox potentials of $^{\bullet}OH/OH^-$ (1.99 eV), H_2O_2 (1.77 eV) and O_3 (2.07 eV), suggesting that such photocatalysts may have much stronger oxidation abilities.

3.7. Mechanism for the enhancement of the photocatalytic activity of BiOI by Ag

Although silver can enhance the activity of many photocatalysts, such as TiO_2 and ZnO [19–21,42], there is no report about the Ag/BiOI photocatalyst. It is well known, photocatalytic process is mainly based the generation and separation of the photoinduced electron–hole pairs. If photoinduced e^-/h^+ can be separated

Table 2
Pseudo first-order rate constants of the catalytic photodecomposition of different dyes.

Catalyst	Acid orange II		Methyl orange		Rhodamine B	
	K (h^{-1})	R	K (h^{-1})	R	K (h^{-1})	R
BiOI	0.1594	0.9972	0.0843	0.9691	0.0502	0.9990
0.3%Ag/BiOI	0.4036	0.9968	0.2641	0.9843	0.1313	0.9982
0.6%Ag/BiOI	0.6377	0.9982	0.3361	0.9968	0.1703	0.9996
0.9%Ag/BiOI	0.3386	0.9987	0.1780	0.9969	0.0928	0.9991

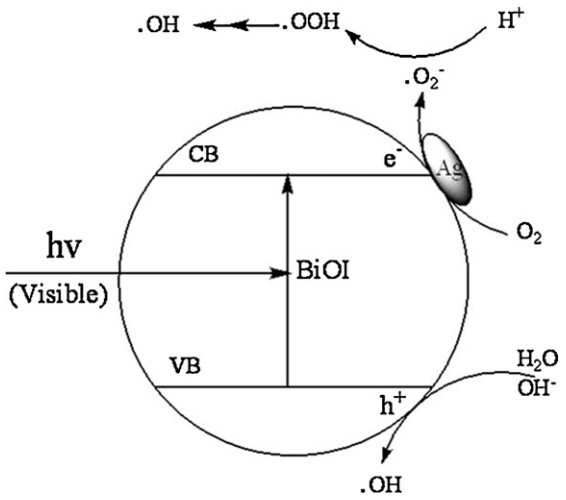

Fig. 10. The suggested mechanism of the photocatalytic activity improvement of Ag/BiOI.

effectively, it is benefited to the photocatalytic activities. When coupling BiOI with metallic Ag, photogenerated electrons transfered to metallic Ag, which had a significant effect on charge separation. And the XPS analysis indicates that silver valence state is zero in Ag/BiOI samples. According to the above analysis, we proposed a mechanism to illustrate possible charge separation process (see Fig. 10). Under visible excitation, the electron of BiOI can be promoted from the valence band to the conduction band, leaving behind a hole in the valence band. Then the electron transfer to metallic silver particles because the Fermi level of BiOI is higher than that of silver metals. This results in the formation of Schottky barrier at metal-semiconductor contact region, which improves the charge separation. In the photocatalytic process, the photogenerated electrons accumulated on the surface of Ag had good fluidity and could be transferred to surface-absorbed oxygen rapidly to form activated $^{\bullet}O_2^-$ [43]. The activated $^{\bullet}O_2^-$ further produces $^{\bullet}OH$ via a series of reaction with H^+. This step is the photoreduction process. On the other hand, holes accumulated at the valence band of BiOI could also react with H_2O to give rise to hydroxyl radical $^{\bullet}OH$, which is the photooxidation process. Both the photoreduction and photooxidation step generate $^{\bullet}OH$ which is responsible for the degradation of pollutant. All photocatalytic reactions are summarized in the following equations ((4)–(10)):

$$BiOI \xrightarrow{h\nu} BiOI(e_{cb}^- - h_{vb}^+) \quad (4)$$

$$e_{cb}^- + Ag \rightarrow Ag(e_{cb}^-) \quad (5)$$

$$Ag(e_{cb}^-) + O_2 \rightarrow O_2^- \quad (6)$$

$$\cdot O_2^- + H^+ \rightarrow \cdot OOH \rightarrow \cdot OH \quad (7)$$

$$H_2O + h_{vb}^+ \rightarrow \cdot OH + H^+ \quad (8)$$

$$OH^- + h_{vb}^+ \rightarrow \cdot OH \quad (9)$$

$$e_{cb}^- + h_{vb}^+ \rightarrow \text{heat} \quad (10)$$

Besides, the surface plasmon resonance of Ag metals on BiOI is excited by visible light (see Fig. 6), enhancing the surface electron excitation and interfacial electron transfer [34–36]. The excitation of plasmon resonance can also contribute to the enhancement in the photocatalytic activity under visible light irradiation, as reported for Ag–TiO_2 [36], Au–TiO_2 [44] and Pt–TiO_2 [45]. Thus, we suggest that the cooperative effects of Ag deposits according to the above two mechanisms lead to the significant enhancement in the BiOI photocatalytic activity under visible light irradiation.

The silver content has also influenced the efficiency of electron–hole separation. It is found that the 0.6% Ag content is optimum to achieve the highest efficiency of the dyes photodegradation. More Ag content (0.9%) is detrimental to the photodegradation efficiency. It may be explained that at the Ag content below its optimum value, the Ag particles deposited on the BiOI surface can act as electron–hole separation centers, and facilitate the interfacial electron transfer to dioxygen or other electron acceptors. On the contrary, when the Ag content above its optimum value, too many negatively charged Ag particles can capture holes and become the recombination centers, which has been confirmed by the results of PL. Meanwhile, the excessive silver can result in the agglomeration of silver nanoparticles on the surface of BiOI, which will cause the loss of surface area and scatter visble light [46], lowering the photoquantum efficiency of the photocatalytic reaction.

4. Conclusions

In summary, a series of novel Ag/BiOI catalysts with excellent photocatalytic performance were successfully prepared through a hydrothermal process combined with a photodeposited method. Due to the deposition of silver, Ag/BiOI showed substantial improvement in the photocatalytic activity for the degradation of dyes under visible light irradiation. The loaded Ag nanoparticles on BiOI could form Schottky barrier between their contact regions, which enhanced the surface electron excitation and electron–hole separation, thus promoting the photocatalytic activity. In addition, the surface plasmon resonance of Ag metals on BiOI excited by visible light could also contribute to the enhancement in the photocatalytic activity. It is suggested that Ag/BiOI catalysts are promising visible-light-driven photocatalysts for environmental applications.

Acknowledgments

The authors gratefully acknowledge Shanghai Municipal Commission of Education (11YZ15), Shanghai Leading Academic Disciplines (S30109), National Natural Science Foundation of China (50971085), Shanghai Science & Technology Committee (09JC1406100) and the Program for Professor of Special Appointment in Shanghai (Eastern Scholar) for the financial support.

References

[1] F. Han, V.S.R. Kambala, M. Srinivasan, D. Rajarathnam, R. Naidu, Appl. Catal. A. 359 (2009) 25–40.
[2] S. Malato, P. Fernandez-Ibanez, M.I. Maldonado, J. Blanco, W. Gernjak, Catal. Today 147 (2009) 1–59.
[3] R. Asahi, T. Morikawa, T. Ohwaki, K. Aoki, Y. Taga, Science 293 (2001) 269–271.
[4] M.A. Shannon, P.W. Bohn, M. Elimelech, J.G. Georgiadis, B.J. Marinas, A.M. Mayes, Nature 452 (2008) 301–310.
[5] J.C. Yu, W.K. Ho, J.G. Yu, H.Y. Yip, P.K. Wang, J.C. Zhao, Environ. Sci. Technol. 39 (2005) 1175–1179.
[6] S. Kim, S.J. Hwang, W.Y. Choi, J. Phys. Chem. B 109 (2005) 24260–24267.
[7] X. Shu, Z. An, L. Wang, J. He, Chem. Commun. 39 (2009) 5901–5903.
[8] F. Chen, W. Zou, W. Qu, J. Zhang, Catal. Commun. 10 (2009) 1510–1513.
[9] W. Wang, J. Zhang, F. Chen, D. He, M. Anpo, J. Colloid Interface Sci. 323 (2008) 182–186.
[10] K. Nagaveni, M.S. Hegde, N. Ravishankar, G.N. Subbanna, G. Madrad, Langmuir 20 (2004) 2900–2907.
[11] W. Zhao, W.H. Ma, C.C. Chen, J.C. Zhao, Z.G. Shuai, J. Am. Chem. Soc. 16 (2004) 4782–4783.
[12] W.D. Wang, F.Q. Huang, X.P. Lin, J.H. Yang, Catal. Commun. 9 (2008) 8–12.
[13] S.Y. Chai, Y.J. Kim, M.H. Jung, A.K. Chakraborty, D. Jung, W.I. Lee, J. Catal. 262 (2009) 144–149.
[14] W.D. Wang, F.Q. Huang, X.P. Lin, Scripta Mater. 56 (2007) 669–672.
[15] Z. Deng, D. Chen, B. Peng, F. Tang, Cryst. Growth Des. 8 (2008) 2995–3003.
[16] X. Zhang, Z.H. Ai, F.L. Jia, L.Z. Zhang, J. Phys. Chem. C 112 (2008) 747–753.
[17] X. Zhang, L.Z. Zhang, T.F. Xie, D.J. Wang, J. Phys. Chem. C 113 (2009) 7371–7378.
[18] R. Costi, A.E. Saunders, E. Elmalem, A. Salant, U. Banin, Nano Lett. 8 (2008) 637–641.

[19] Y.H. Zheng, C.Q. Chen, Y.Y. Zhan, X.Y. Lin, Q. Zheng, K.M. Wei, J.F. Zhu, Phys. Chem. C 112 (2008) 10773–10777.
[20] Y.H. Zheng, L.R. Zheng, C.Q. Chen, Y.Y. Zhan, X.Y. Lin, Q. Zheng, K.M. Wei, Inorg. Chem. 46 (2007) 6980–6986.
[21] Z.C. Shan, J.J. Wu, F.F. Xu, F.Q. Huang, H.P. Ding, J. Phys. Chem. C 112 (2008) 15423–15428.
[22] F.X. Zhang, N.J. Guan, Y.Z. Li, X. Zhang, J.X. Chen, H.S. Zeng, Langmuir 19 (2003) 8230–8234.
[23] I.M. Arabatzis, T. Stergiopoulos, M.C. Bernard, D. Labou, S.G. Neophytides, P. Falaras, Appl. Catal. B 42 (2003) 187–201.
[24] Z.H. Ai, Z.H. Ho, S.C. Lee, L.Z. Zhang, Environ. Sci. Technol. 43 (2009) 4143–4150.
[25] K. Gurunathan, Int. J. Hydrogen Energy. 29 (2004) 933–940.
[26] K.L. Zhang, C.M. Liu, F.Q. Huang, C. Zheng, W.D. Wang, Appl. Catal. B 68 (2006) 125–129.
[27] L.A. Brook, P. Evans, H.A. Foster, M.E. Pemble, A. Steele, D.W. Sheel, H.M. Yates, J. Photochem. Photobiol. A 187 (2007) 53–63.
[28] W.E. Morgan, J.R. Vanwazer, W.J. Stec, J. Am. Chem. Soc. 95 (1973) 751–755.
[29] M. Shao, L. Lu, H. Wang, S. Wang, M. Zhang, D. Ma, S. Lee, Chem. Commun. 28 (2008) 2310–2312.
[30] R. Priya, K.V. Baiju, S. Shukla, S. Biju, M.L.P. Reddy, K. Patil, K.G.K. Warrier, J. Phys. Chem. C 113 (2009) 6243–6255.
[31] W. Su, S.S. Wei, J.X. Tang, J. Hazard. Mater. 172 (2009) 716–720.
[32] E. Stathatos, P. Lianos, P. Falaras, A. Siokou, Langmuir 16 (2000) 2398–2400.
[33] J. Yu, J. Xiong, B. Cheng, S. Liu, Appl. Catal. B 60 (2005) 211–221.
[34] G. Lassaletta, A.R. Gonzales-Elipe, A. Justo, A. Fernandez, F.J. Ager, M.A. Respaldiza, J.G. Soares, M.F. Da Silva, J. Mater. Sci. 31 (1996) 2325–2332.
[35] A.M. Schwartzberg, J.Z. Zhang, J. Phys. Chem. C 112 (2008) 10323–10337.
[36] M.K. Seery, R. George, P. Floris, S.C. Pillai, J. Photochem. Photobiol. A 189 (2007) 258–263.
[37] J. Henle, P. Simon, A. Frenzel, S. Scholz, S. Kaskel, Chem. Mater. 19 (2007) 366–373.
[38] Y.H. Zheng, C.Q. Chen, Y.Y. Zhan, X.Y. Lin, Q. Zheng, K.M. Wei, J.F. Zhu, Inorg. Chem. 46 (2007) 6675–6682.
[39] J. Tang, J. Ye, Chem. Phys. Lett. 410 (2005) 104–107.
[40] M.A. Butler, D.S. Ginley, J. Electrochem. Soc. 125 (1978) 228–232.
[41] X.P. Lin, J.C. Xing, W.D. Wang, Z.C. Shan, F.F. Xu, F.Q. Huang, J. Phys. Chem. C 111 (2007) 18288–18293.
[42] L. Sun, J. Li, C.L. Wang, S.F. Li, Y.K. Lai, H.B. Chen, C.J. Lin, J. Hazard. Mater. 171 (2009) 1045–1050.
[43] S.X. Liu, Z.P. Qu, X.W. Han, C.L. Sun, Catal. Today 93-95 (2004) 877–884.
[44] X.Z. Li, F.B. Li, Environ. Sci. Technol. 35 (2001) 2381–2387.
[45] Y. Cho, W. Choi, J. Photochem. Photobiol. A. 148 (2002) 129–135.
[46] H.M. Sung-Suh, J.R. Choi, H.J. Hah, S.M. Koo, Y.C. Bae, J. Photochem. Photobiol. A 163 (2004) 37–44.